CCS Chemistry

RESEARCH ARTICLE

Received: Jan. 6, 2024 | Accepted: Apr. 2, 2024 | Published: Apr. 30, 2024

High-Intensity Focused Ultrasound-Induced Disulfide Mechanophore Activation in Polymeric Nanostructures for Molecule Release

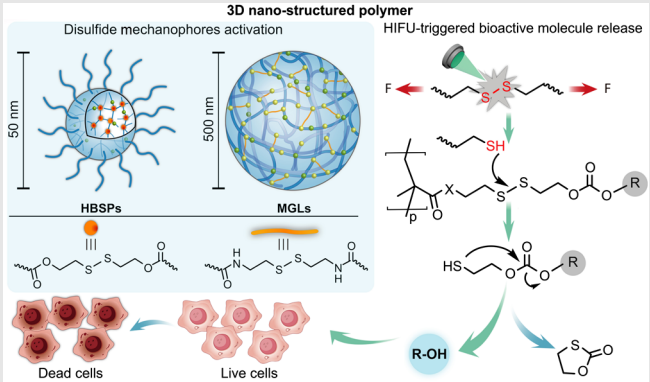
Jilin Fan[1,2], Kuan Zhang[1,2,3], Mingjun Xuan[1,2]*, Xiang Gao[1,2], Rostislav Vinokur[1], Robert Göstl[1,2], Lifei Zheng[3]* & Andreas Herrmann[1,2]*

[1]*DWI—Leibniz Institute for Interactive Materials, 52056 Aachen,* [2]*Institute of Technical and Macromolecular Chemistry, RWTH Aachen University, 52074 Aachen,* [3]*Wenzhou Institute, University of Chinese Academy of Sciences, 325001 Wenzhou*

**Corresponding authors: xuan@dwi.rwth-aachen.de; zhenglf@ucas.ac.cn; herrmann@dwi.rwth-aachen.de*

Cite this: *CCS Chem.* **2024**, 6, 1895–1907
DOI: 10.31635/ccschem.024.202403876

Ultrasound (US) activation of mechanophores in polymers that initiates cascade chemical reactions is a promising strategy for on-demand molecule release. However, the typical US frequency used for mechanochemistry is around 20 kHz, producing inertial cavitation that exceeds the tolerance threshold of biological systems. Here, high-intensity focused US (HIFU) as a mechanical stimulus is introduced to drive the activation of disulfide mechanophores in hyperbranched star polymers (HBSPs) and microgels (MGLs). The mechanism of molecular release is attributed to the thiol-disulfide exchange reaction and subsequent intramolecular cyclization. We reveal that HBSPs and MGLs effectively transduce HIFU as mechanical input to chemical output, demonstrated by the quantification of the release of fluorescent umbelliferone (UMB). Moreover, an in vitro study of drug release is carried out using camptothecin as the model drug, which is covalently loaded in MGLs, demonstrating the potential of our system for controlled drug delivery to cancer cells.



Keywords: mechanophores, polymer mechanochemistry, polymeric nanostructures, ultrasound, drug release, sonopharmacology

Introduction

Polymer mechanochemistry strives to control chemical transformations by rearranging or cleaving specific bonds at precisely defined sites within polymer chains. Mechanical forces, such as tension and compression, or indirect sources, such as US, are being used.[1–4] The force-sensitive moieties responsible for this process are known as mechanophores.[5–9] The development of diverse mechanophores has expanded the possibilities for designing polymer systems with tailored mechanochemical properties.[10–16] While polymer mechanochemistry has found widespread applications in polymer science ranging from damage detection,[17–19] stress sensing,[20–22] and

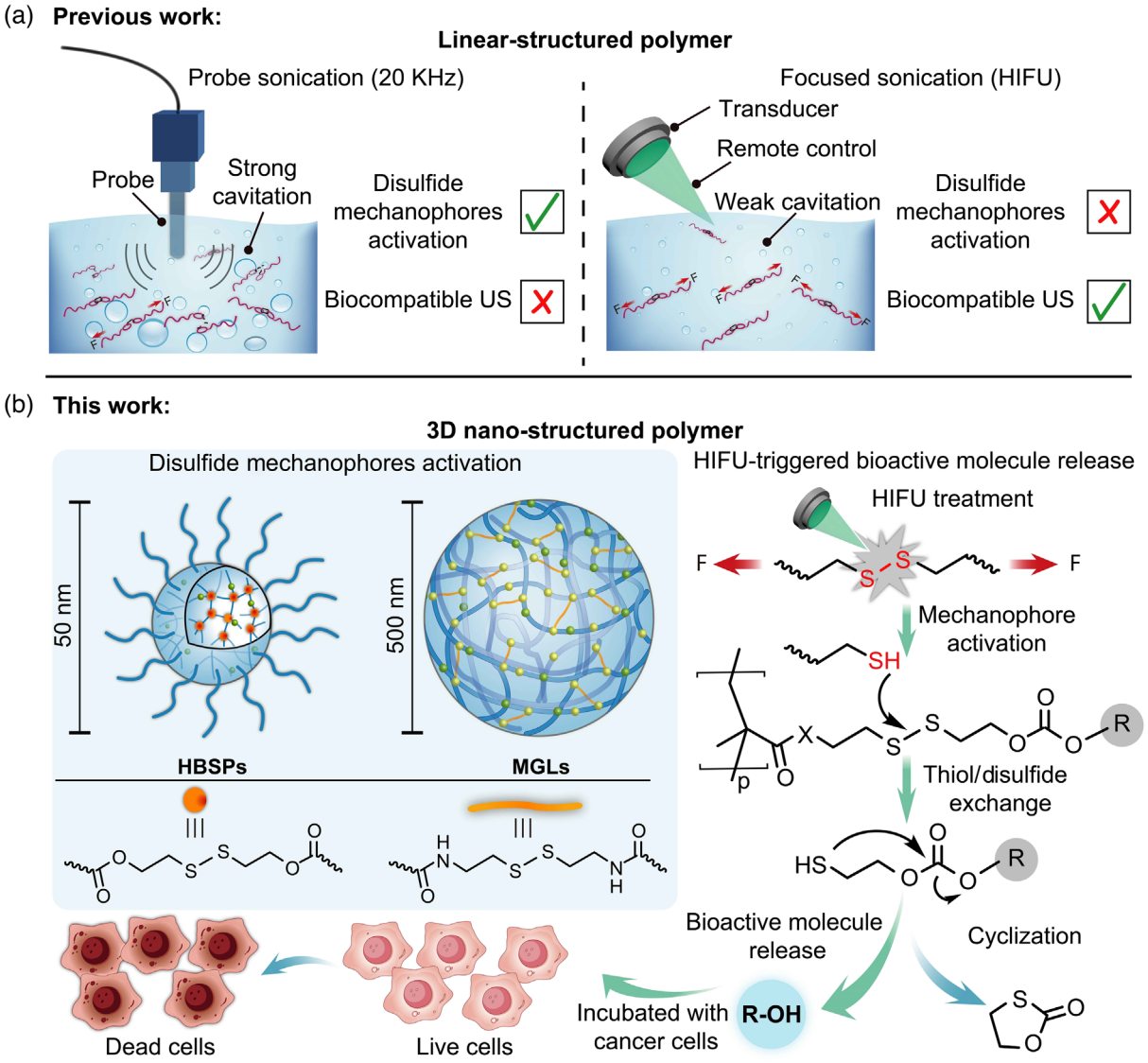


Figure 1 | *(a) Summary of previous work on US-activated LP structures containing disulfide mechanophores. (b) Schematic illustration of the mechanism of disulfide mechanophores activation in branched and cross-linked polymeric structures upon HIFU irradiation involving thiol-disulfide exchange reactions and the following intramolecular cyclization.*

nanolithography[4] to self-regulating materials,[23] its utilization in a biomedical context is still in an early stage.

Recently, our group[24-30] and others[31-33] has pioneered the field termed sonopharmacology, which encompasses the application of principles of polymer mechanochemistry for pharmacotherapy.[34] Indeed, the deep penetration of US in biological tissues offers the possibility of achieving mechanochemical processes in biological systems with precise spatiotemporal control. This capability provides a valuable framework for manipulating the activation and release of drug molecules.[35,36] However, conventional polymer mechanochemistry initiated by 20 kHz US poses a risk of damaging cells and tissues due to the strong cavitation effect and the formation of liquid microjets.[37] In contrast, high-intensity focused US (HIFU) with MHz frequency has been proven to be biocompatible and is commonly associated with biomedical applications.[38] Among these, Li and coworkers[32] have reported the activation of azo mechanophores embedded in hydrogels by HIFU to generate free radicals for noninvasive cancer therapy. More recently, Robb and coworkers[33] developed a seminal synergistic platform that combines the selective activation of masked 2-furylcarbinol mechanophores in linear polymers (LPs) with biocompatible focused US using pressure-sensitive gas vesicles (GVs) as acousto-mechanical transducers. Although this approach allows for precise control over the release of drug molecules, it necessitates systemic coinjection and colocalization of the GVs and polymers in tumor tissues, which might add complexity to practical

DOI: 10.31635/ccschem.024.202403876
Citation: *CCS Chem.* **2024**, 6, 1895–1907
Link to VoR: https://doi.org/10.31635/ccschem.024.202403876

implementation of this technique. Therefore, further research is needed to explore the full potential of biocompatible US-based polymer mechanochemistry for the development of drug delivery systems.

Disulfide mechanophores have recently attracted significant interest due to their low bond dissociation energy and thermal stability. They are commonly incorporated into LPs and can be activated in the presence of US irradiation.[24–27,39–44] However, the activation of disulfide mechanophores using HIFU in polymeric nanostructures has been unexplored. In this study, we present the design of hyperbranched star polymers (HBSPs) and microgels (MGLs) containing disulfide mechanophores, as well as inactive fluorescent probes (umbelliferone, UMB) or a small molecule drug (camptothecin, CPT). Within these systems, the disulfide mechanophores are covalently incorporated. Upon HIFU irradiation, the disulfide mechanophores undergo bond scission, generating free thiols. These, in turn, activate a carbonate unit within the polymer scaffolds through thiol-disulfide exchange and intramolecular cyclization, resulting in the release of UMB or CPT (Figure 1a,b). By exposing HeLa cells to the released drug, we can further investigate their cytotoxic effects and potential for cancer treatment. Overall, this work demonstrates the potential of HIFU as a noninvasive method for triggering drug release from polymeric nanomaterials.

Experimental Methods

Materials

All chemical reagents and solvents were used without further purification unless otherwise stated. 2-Hydroxyethyl disulfide (technical grade, Sigma-Aldrich, Steinheim, Baden-Württemberg, Germany), methacryloyl chloride (97%, Sigma-Aldrich), triethylamine (TEA, ≥99%, Sigma-Aldrich), tetrahydrofuran (THF, anhydrous, Sigma-Aldrich), dichloromethane (anhydrous, ≥99.8%, Sigma-Aldrich), *N*,*N*′-disuccinimidyl carbonate (≥95%, Sigma-Aldrich), toluene (≥99.5%, Sigma-Aldrich), 4-(dimethylamino)pyridine (>99.0%, TCI Deutschland GmbH, Eschborn, Hesse, Germany), 1,4-dioxane (99.8%, Sigma-Aldrich), triphosgene (98%, Sigma-Aldrich) UMB (99%, ACROS ORGANICS, Bvba, Antwerp, Belgium), CPT (≥95%, Abcr GmbH, Karlsruhe, Baden-Württemberg, Germany), 4-cyano-4-(phenylcarbonothioylthio)pentanoic acid (reversible addition fragmentation chain-transfer (RAFT) agent, Sigma-Aldrich), *N*,*N*-diisopropylethylamine (≥99%, Sigma-Aldrich), $CuBr_2$ (99%, Sigma-Aldrich), Me_6TREN (97%, Sigma-Aldrich), cystamine dihydrochloride (≥97.0%, TCI Deutschland GmbH), 2-mercaptoethanol (MCE, >99.0%, TCI Deutschland GmbH), and bis[2-(2′-bromoisobutyryloxy)ethyl]disulfide (98%, Sigma-Aldrich) were used as received. Pentafluorophenyl methacrylate (PFPMA, 97%, Abcr GmbH) and poly(ethylene glycol) methyl ether methacrylate (PEGMEMA, M_n ~ 300 Da, Sigma-Aldrich) were purified by a column of activated basic Al_2O_3 to remove the inhibitor before utilization. 2,2′-Azobis(2-methylpropionitrile) (98.0%) was obtained from Sigma-Aldrich and recrystallized twice from MeOH. Dialysis membranes (3.5 kDa MWCO) were obtained from Spectrum Labs (Rancho Dominguez, California, USA). The centrifugal filter (3000 MWCO) was obtained from Sartorius (Göttingen, Lower Saxony, Germany). The HeLa cell line was obtained from ATCC (Manassas, Virginia, USA): The Global Bioresource Center. Ultrapure Milli-Q water (18.2 MΩ · cm) was used.

Analytical instrumentation

^{1}H and ^{13}C NMR spectra were measured at room temperature in $CDCl_3$ with a 400 MHz Bruker Avance 400 spectrometer (Bruker, Billerica, Massachusetts, USA; ^{13}C: 101 MHz). The chemical shifts are reported in δ units using residual protonated solvent signals as the internal standard (^{1}H: $CDCl_3$ ($^\delta$H = 7.26 ppm), ^{13}C: $CDCl_3$ ($^\delta$C = 77.16 ppm)). Thin-layer chromatography (TLC) was performed on a Merck TLC Silica gel 60 F_{254} TLC plates (Merck KGaA, Darmstadt, Hesse, Germany) with a fluorescence indicator, employing a 254 nm or 365 nm UV hand lamp for visualization. Silica gel (40–63 μm) for chromatography was used for flash column chromatography. Gel permeation chromatography/size exclusion chromatography (GPC/SEC) with THF [high-performance liquid-chromatography (HPLC) grade] was performed using a HPLC pump (PU-2080plus, Jasco, Hachioji, Tokyo, Japan) equipped with a refractive index (RI) detector (RI-2031plus, Jasco). The sample solvent contained 250 mg/mL 3,5-di-*t*-4-butylhydroxytoluene (≥99%, Fluka Chemie GmbH, Buchs, St. Gallen, Switzerland) as the internal standard. One precolumn (8 × 50 mm) and four SDplus gel columns (8 × 300 mm, MZ Analysentechnik GmbH, Mainz, Rhineland-Palatinate, Germany) were applied at a flow rate of 1.0 mL min^{-1} at 20 °C. The diameter of the gel particles was 5 μm, the nominal pore widths were 50, 102, 103, and 104 Å. Calibration was achieved using narrowly distributed poly(methyl methacrylate) (PMA) standards (polymer standards service (PSS)). Molar masses (M_n and M_w) and molar mass distributions (M_w/M_n) were calculated by using the PSS WinGPC UniChrom software (Version 8.1.1; Mainz, Rhineland-Palatinate, Germany). Ultrahigh performance liquid-chromatography-mass spectrometer (UHPLC-MS) system: ACQUITY UPLC I-Class System (Waters, Milford, Massachusetts, USA) with the compatible ACQUITY UPLC PDA eλ Detector and ACQUITY QDa detector (Waters). Solvents: A = water [contained 0.1% trifluoroacetyl (TFA)], B = acetonitrile (contained 0.1% TFA); flow = 0.4 mL min^{-1}; gradient (B): 0–1 min (10%), 1–5 min (10%–90%), 5–7 min (90%), 7–10 min (90%–10%). Electrospray ionization mass spectrometry (ESI MS): micrOTOF-Q II™ ESI-Qq-TOF mass spectrometer system

DOI: 10.31635/ccschem.024.202403876
Citation: *CCS Chem.* **2024**, 6, 1895–1907
Link to VoR: https://doi.org/10.31635/ccschem.024.202403876

(BRUKER, Billerica, Massachusetts, USA). Transmission electron microscopy (TEM) images were captured on a LIBRA®120 transmission electron microscope (Carl Zeiss, Oberkochen, Baden-Württemberg, Germany) with an accelerating voltage of 120 kV, and images were recorded using a Gatan Ultra Scan 1000 (Gatan Incorporation, Pleasanton, California, USA). TEM sample preparation: one drop (~10 μL) of sample was deposited onto a carbon-coated copper grid and then air-dried. Dynamic light scattering (DLS) was measured on a Zetasizer instrument (Zetasizer Ultra, Malvern, Worcestershire, United Kingdom). Samples were dispersed in H_2O/DMSO (4:1, v/v), and then the mixture was transferred to a disposable plastic cell.

Fluorescence spectroscopy

Fluorescence spectroscopy was performed on a SpectraMax iD3 spectrometer (Molecular Devices, San Jose, California, USA) at room temperature. For fluorescence spectra measurements of HBSPs and MGLs-UMB, samples were excited at 325 nm. The spectral bandwidths were set to 1 nm (370 ~ 600 nm) for emission. To obtain the standard curve of UMB, the fluorescence value was collected at the emission wavelength of 465 nm. For fluorescence spectra measurements of MGLs-CPT, samples were excited at 335 nm. The spectral bandwidths were set to 2 nm (375 ~ 610 nm) for emission. To obtain the standard curve of CPT, the fluorescence value was collected at the emission wavelength of 449 nm. The integration time was 0.1 s, and all spectroscopic measurements were carried out with a pureGrade™ 96-well plate purchased from BRAND GmbH (Frankfurt, Hesse, Germany). For the sonicated solution of HBSPs or MGLs, filtration steps were needed before the fluorescence measurements. Filtration was carried out as follows: Centrifugation three times at 10,000 rpm (10 min); then the suspensions were filtered through a centrifugal filter (3000 MWCO) by centrifugation at 5000 rpm.

Sonication experiments

Sonication experiments were performed with a home-built HIFU setup. The core devices include waveform generator (33511B, Keysight Technologies, Santa Rosa, California, USA), RF amplifier (AG1021, T&C Power Conversion, Inc., Rochester, New York, USA), and transducers (0.66 MHz, 1.5 MHz and 2.5 MHz, Precision Acoustics Ltd., Dorchester, Dorset, United Kingdom). A 0.5 mm needle hydrophone (Precision Acoustics Ltd., UK) was used for locating the transducer focal point. A custom-made motorized 3D-manipulator/positioning system for controlling the well plate submerged in water was employed. Pulsed sonication (2 s on, 1 s off) was used. 10 mg of polymer were dissolved in 1 mL mixture of H_2O/DMSO (4:1, v/v). 1 mL of this solution was added into the 24-well plate with a transparent base made from ultrathin film (lumox® multiwall 24, SARSTEDT, Nümbrecht, North Rhine-Westphalia, Germany). Then, the well plate was placed in the well plate holder. Samples were exposed to constant sonication for a certain time. The samples were then kept for 72 h to complete the downstream release reactions at room temperature before the fluorescence measurements.

Cell imaging

HeLa cells used for imaging were cultured in Dulbecco's modified Eagle's Medium (DMEM) containing 10% heat-inactivated fetal bovine serum (FBS) supplemented with 100 U mL^{-1} of penicillin and 100 μg mL^{-1} streptomycin at 37 °C under a humidified atmosphere containing 5% CO_2. The HeLa cells were seeded in an ibidi μ-Slide 8 Well (with glass bottom) at a density of 2.5×10^5 cells per well in 500 μL culture medium. After 24 h, HeLa cells were incubated with different concentrated sonicated samples or nonsonicated samples in phosphate-buffered saline (PBS) at 37 °C, then washed with PBS three times. Then, PBS was added into the wells (500 μL per well), and 2 μL (1 mg mL^{-1}) calcein acetomethoxy (AM) and 2 μL (1 mg mL^{-1}) propidium iodide (PI) were transferred to the wells and mixed for 5 min. PBS was used to wash out the free cell imaging agents. Then the fluorescence imaging of cells was performed on a confocal laser scanning microscope (STP8, Leica, Wetzlar, Hesse, Germany) (confocal excitation: Calcein AM: 496 nm, PI: 561 nm) and analyzed by ImageJ.

MTS proliferation assays

HeLa cells were used to evaluate the cytotoxicity of different samples. HeLa cells were cultured in a basal medium containing DMEM (supplemented with 10% FBS and 1% antibiotics/antimycotics) at 37 °C. Actual cell viability was monitored by using a tetrazolium compound 3-(4,5-dimethylthiazol-2-yl)-5-(3-carboxymethoxyphenyl)-2-(4-sulfophenyl)-2H-tetrazolium (inner salt, MTS reagent) and a chemical electron acceptor dye (phenazine ethosulfate) (Promega, Germany), using an assay according to the manufacturer's instructions. Briefly, approximately 5000 cells in 100 μL of medium were seeded into 96-well plates. After overnight incubation, the culture medium in the 96-well plates was removed and exchanged with fresh medium (100 μL) containing different concentrated testing samples. Control cultures were treated with dimethyl sulfoxide (DMSO) alone. The final concentration of DMSO in the medium did not exceed 0.5%. After 48 h incubation, the cell culture media were removed, the cells were washed with 100 μL PBS buffer, and then 20 μL MTS reagent with 100 μL fresh medium was added to the cells. The mixture of MTS reagent with cell culture medium served as negative control. The resulting solution was mixed thoroughly, and the absorbance was monitored using a microplate spectrophotometer at 490 nm (Synergy™ HT microplate

DOI: 10.31635/ccschem.024.202403876
Citation: *CCS Chem.* **2024**, 6, 1895–1907
Link to VoR: https://doi.org/10.31635/ccschem.024.202403876

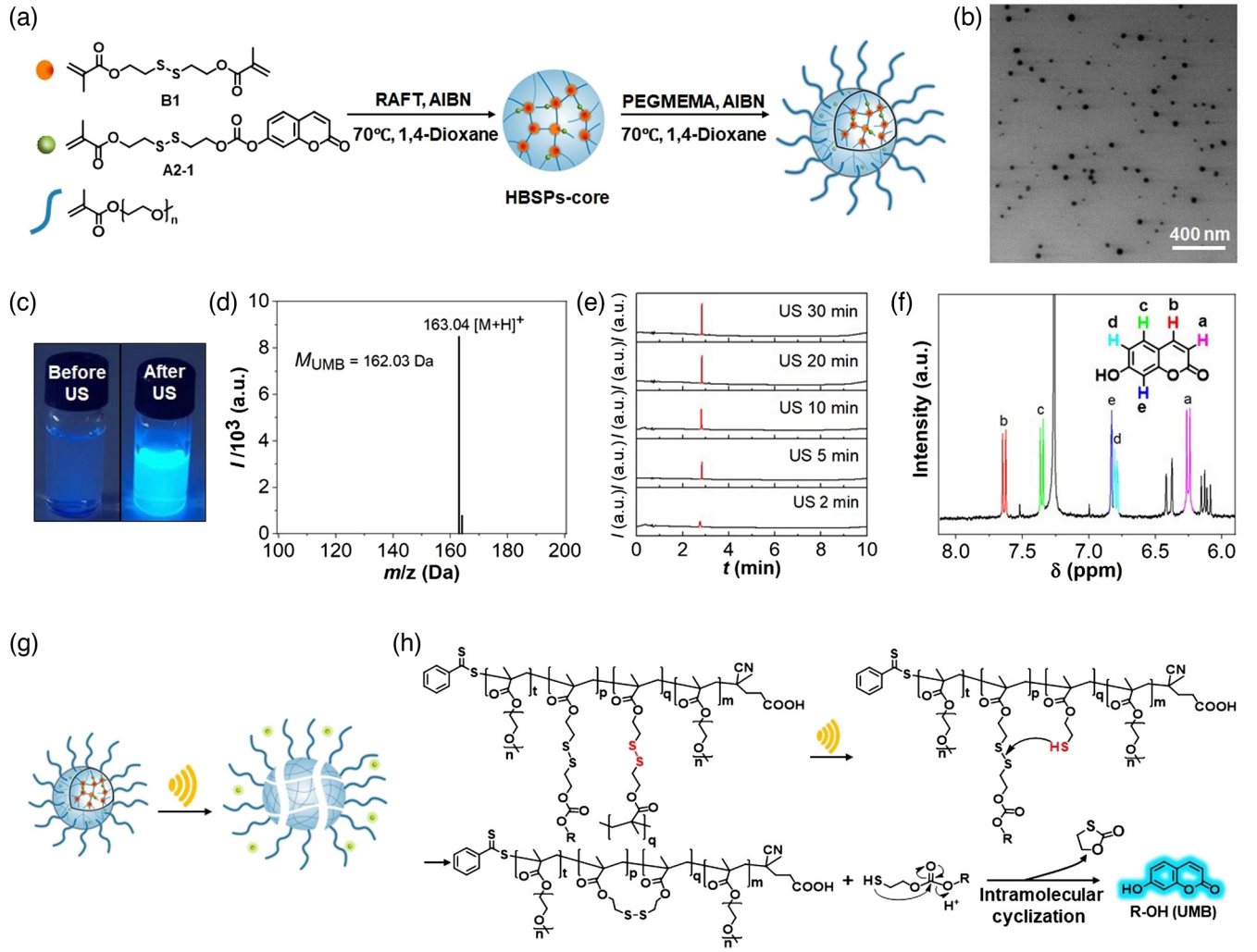


Figure 2 | *Synthesis and characterization of HBSPs, and HIFU-induced disulfide mechanophore activation. (a) RAFT polymerization of PEGMEMA, **A2-1**, and **B1** for the synthesis of HBSPs-core, followed by chain extension on HBSPs-core surface with PEGMEMA. (b) TEM micrograph of HBSPs. (c) Photograph of HBSPs solutions under 365 nm UV light irradiation before and after HIFU treatment (f = 1.5 MHz, 2 s on, 1 s off, 30 min, 3 d equilibration). (d) Mass spectrometry of released UMB after HIFU treatment. The molar mass of UMB at 163.04 Da was retrieved. (e) UPLC elugrams of released UMB with a retention time of 2.82 min. (f) Excerpt from ^{1}H NMR spectrum of released UMB (400 MHz, $CDCl_3$). Color-coded signals represent the characteristic peaks of UMB. (g) Schematic of the degradation of HBSPs under HIFU irradiation. (h) The mechanism of HIFU-induced disulfide scission and subsequent intramolecular reaction pathway for activating disulfide mechanophores and fluorescent UMB release.*

reader, BioTek Instruments, Winooski, Vermont, USA). MTS signals were used for survival and proliferation determination. All the sample cultures were performed at least in triplicate.

Results and Discussion

HBSPs synthesis and HIFU-induced disulfide mechanophore activation

Initially, we assessed whether cargo molecules could be released from the disulfide-carbonate structure. Therefore, the monomer containing a disulfide, carbonate, and an UMB unit (**A2-1**) as well as a model compound containing only a hexanol, carbonate, and UMB unit (**A3**) were synthesized (Supporting Information Scheme S1). UMB was the designated fluorescent reporter, allowing facile quantification of molecule release. In compound **A2-1**, a carbonate linker was positioned in the β-position to the disulfide moiety. Upon thiol-initiated thiol-disulfide exchange and the following intramolecular cyclization, UMB was released, and its fluorescence was turned on due to breakage of the carbonate linker. As shown in Supporting Information Figures S1, S5, and S6, strong fluorescence of **A2-1** solution was observed under 365 nm UV light irradiation after the addition of MCE, indicating

DOI: 10.31635/ccschem.024.202403876
Citation: *CCS Chem.* **2024**, 6, 1895–1907
Link to VoR: https://doi.org/10.31635/ccschem.024.202403876

the occurrence of the thiol-disulfide exchange reaction, followed by the intramolecular cyclization (Supporting Information Scheme S2). The formation of the released fluorescent UMB was further confirmed by ^{1}H NMR spectroscopy and ultrahigh-performance liquid chromatography (UPLC) (Supporting Information Figures S3 and S4). As a control sample, **A3** without the disulfide group was also mixed with MCE. As expected, the reaction mixture containing **A3** and MCE showed no enhancement of fluorescence (Supporting Information Figures S1 and S2).

Next, HBSPs containing disulfide mechanophores were synthesized by combining RAFT copolymerization and chain extension from the endpoints of the HBSP-core with the biocompatible PEG-analogue PEGMEMA. We hypothesized that chain extension would increase the molar mass of the constructs and facilitate the force transmission from the solvated chain ends to the mechanophore-loaded core. The synthesis involved two steps: the fabrication of the polymeric core architecture and the growth of PEGMEMA chains on the surface of the polymeric core (Figure 2a and Supporting Information Scheme S3). **A2-1** containing UMB fluorophores were copolymerized into the HBSPs structures for monitoring the release process. The molar mass of the HBSPs was roughly estimated to 113 kDa by GPC using a RI detector (Supporting Information Figure S7). The molar ratio of PEGMEMA to **A2-1** was approximately 59:1 (Supporting Information Figure S8), meaning that each HBSP polymer contained between 6 and 7 **A2-1** molecules. The morphology and size distribution of the HBSPs were studied using TEM (Figure 2b and Supporting Information Figure

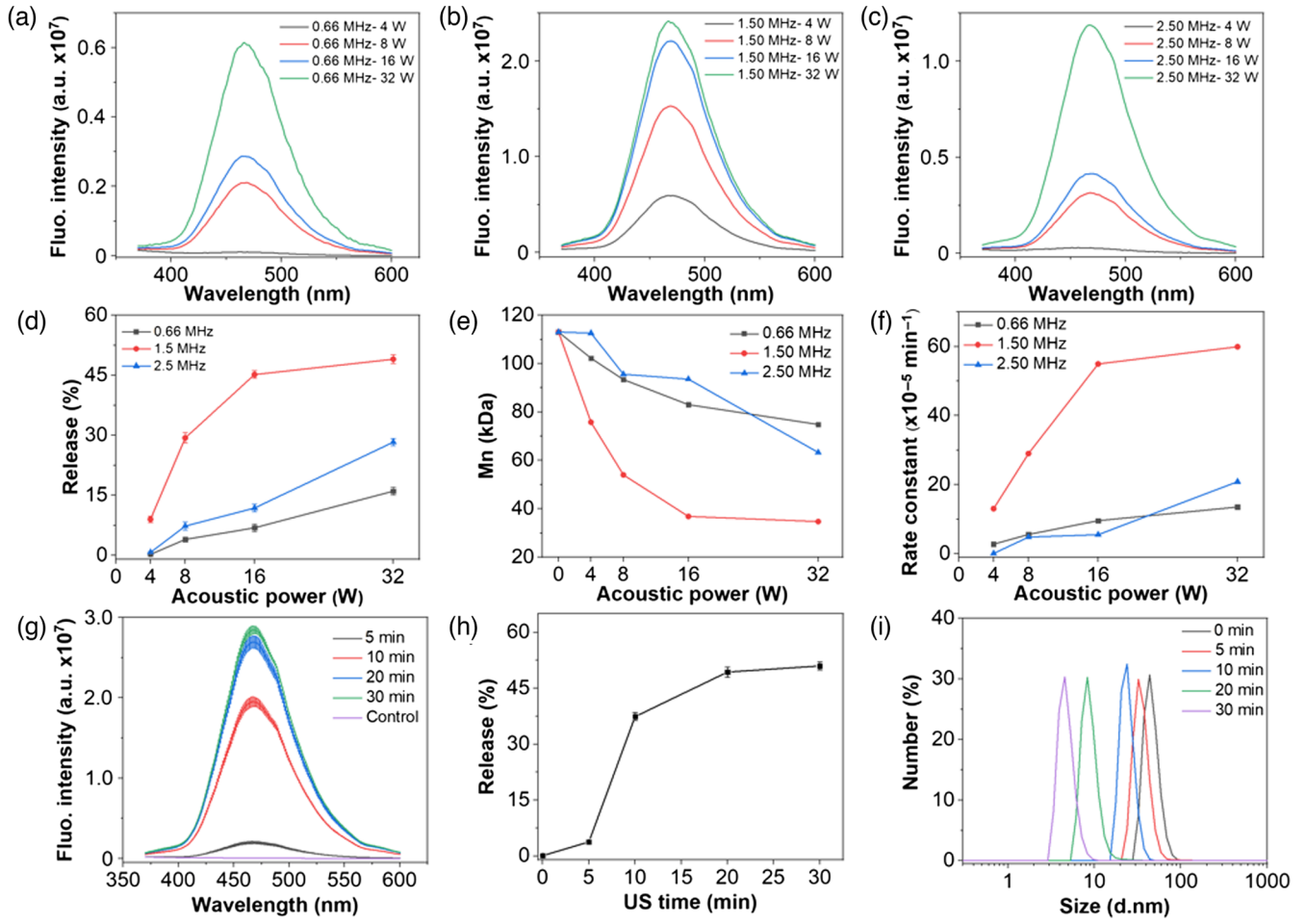


Figure 3 | *Quantification of disulfide mechanophore activation and UMB release using different HIFU parameters. Fluorescence spectra of HBSPs solution after 20 min HIFU irradiation with the frequency of (a) 0.66 MHz, (b) 1.5 MHz, and (c) 2.5 MHz. (d) UMB release from HBSPs with different HIFU frequencies and acoustic power. (e) The change in* M_n *of HBSPs using different HIFU frequencies and acoustic power. (f) The rate constant of HBSPs degradation. (g) Fluorescence spectra of HBSPs solutions after HIFU treatment (1.5 MHz, 32 W) for different durations. (h) The release profile of UMB after HIFU treatment (1.5 MHz) for different durations. (i) Size distribution of HBSPs after HIFU (1.5 MHz, 32 W) treatment for different durations.*

DOI: 10.31635/ccschem.024.202403876
Citation: *CCS Chem.* **2024**, 6, 1895–1907
Link to VoR: https://doi.org/10.31635/ccschem.024.202403876

S9) and DLS, respectively. The diameter of HBSPs was found to be in the range of 20–50 nm (Supporting Information Figures S10 and S11).

Once the HBSPs were obtained, we investigated whether the incorporated disulfide mechanophores could be activated by HIFU. Upon ultrasonication (1.5 MHz, pulse sequence 2 s on, 1 s off) for 30 min, a blue fluorescence from the HBSPs solution was observed (Figure 2c), indicating that the mechanochemical transduction occurred and generated free thiols, which subsequently induced the release of the fluorescent UMB molecules. This was further confirmed by UPLC-MS measurements (Figure 2d,e) and the appearance of characteristic proton peaks of UMB in the ^{1}H NMR spectrum (Figure 2f). The degradation of HBSPs under HIFU irradiation is schematically shown in Figure 2g. In addition, the mechanism of disulfide mechanophore activation and UMB release from HBSPs under HIFU irradiation is illustrated in Figure 2h. To quantify the amount released upon US activation, the fluorescence of sonicated HBSPs solution was measured. The release efficiency was calculated by using the fluorescence of a HBSPs solution that was treated with a large excess of reducing agent MCE as a reference (Supporting Information Figures S15–S17). It was found that the fluorescence intensity increased rapidly in the first 10 min, and the release efficiency of UMB reached the maximum of 49% after 20 min. For comparison, LPs with a molar mass of 48 kDa and a central disulfide mechanophore were synthesized (Supporting Information Scheme S4 and Figures S12 and S13). No fluorescence was detected after 30 min of HIFU treatment (Supporting Information Figure S14), suggesting no activation of the disulfide mechanophore in LPs. This difference can be attributed to the fact that HBSPs have more disulfide scission sites compared to LPs, allowing for a larger number of mechanically active disulfide bonds to facilitate the destruction of HBSPs into fragments for UMB release. Another reason could be the multimechanophore architecture and the higher molar mass of the HBSPs that allows for more efficient transfer of the force to the mechanophores in comparison to linear chain polymers.[45]

Subsequently, the experimental parameters affecting the efficiency of molecule release were systematically investigated. The acoustic power and mechanical index (MI) of the HIFU are detailed in Supporting Information Table S1. At a certain US frequency, the fluorescence intensity of the sonicated HBSPs solutions increased upon enhancing the acoustic power from 4 to 32 W (Figure 3a–c). Moreover, we found that the response sensitivity of HBSPs to 1.5 MHz HIFU was higher compared to 0.66 or 2.5 MHz HIFU. For example, at a power of 32 W, around 50% of UMB, was released under 1.5 MHz HIFU irradiation in 20 min, while increasing the US frequency to 2.5 MHz or decreasing the US frequency to 0.66 MHz decreased the release efficiency to 28% and 16%, respectively (Figure 3d). Additionally, no UMB release was observed from HBSPs when the HIFU acoustic power was lower than 4 W using the output frequencies of 0.66 or 2.5 MHz, whereas 1.5 MHz HIFU still facilitated more than 9% UMB release.

The molar mass and size of HBSPs after HIFU irradiation was also studied using GPC and DLS, respectively. The change in M_n of HBSPs with 0.66, 1.5, and 2.5 MHz HIFU transducers was recorded (Supporting Information Table S2) and plotted against power (Figure 3e). We observed that there was an inversely proportional relationship between M_n and HIFU power.[46,47] The molar mass of HBSPs decreased more rapidly when using the 1.5 MHz HIFU transducer. To determine the degradation rate constants of polymers, kinetic analysis was conducted using a previously reported method (Supporting Information Table S3).[48,49] The rate constant of HBSPs decomposition was plotted as a function of M_n against sonication time. The trend of the rate constant with acoustic power is shown in Figure 3f. Under 1.5 MHz HIFU irradiation, the maximum rate constant was around $60 \cdot 10^{-5}$ min^{-1}, which was higher than those using the other two frequencies. Then, fluorescence intensity measurements were conducted to quantify molecular release at varied HIFU durations using an acoustic power of 32 W (Figure 3g), revealing that more than 50% of fluorescent molecules were released within 30 min sonication (Figure 3h). According to DLS measurements, the size of HBSPs dramatically decreased within 5 min and dropped to less than 10 nm after 20 min, which is consistent with the release kinetics of UMB molecules (Figure 3i and Supporting Information Figure S18).

Synthesis of MGLs-UMB and HIFU-induced disulfide mechanophore activation

Encouraged by the results obtained with HBSPs, we attempted to broaden the carrier scope to MGLs. MGLs-UMB were synthesized in two steps, as illustrated in Figure 4a and Supporting Information Scheme S5. The RAFT polymerization process involved the use of PEGMEMA, PFPMA, and acrylate-disulfide-UMB (**A2-1**) to produce copolymer P1 (Supporting Information Figure S19) with a molecular weight of 12.9 kDa. The molar ratio of PEGMEMA to PFPMA to **A2-1** was approximately 14:5:1 (Supporting Information Figure S20). Each P1 polymer contained approximately two acrylate-UMB molecules. Subsequently, P1 was cross-linked using cystamine to form MGLs-UMB. Notably, the leaving group pentafluorophenolate facilitated the cross-linking reaction, which was characterized by ^{19}F NMR spectroscopy (Supporting Information Figure S21). The morphology and size distribution of MGLs-UMB were examined using TEM imaging (Figure 4b and Supporting Information Figure S22). The MGLs-UMB exhibited a size range of 150–450 nm (Supporting Information Figure S23).

DOI: 10.31635/ccschem.024.202403876
Citation: *CCS Chem.* **2024**, 6, 1895–1907
Link to VoR: https://doi.org/10.31635/ccschem.024.202403876

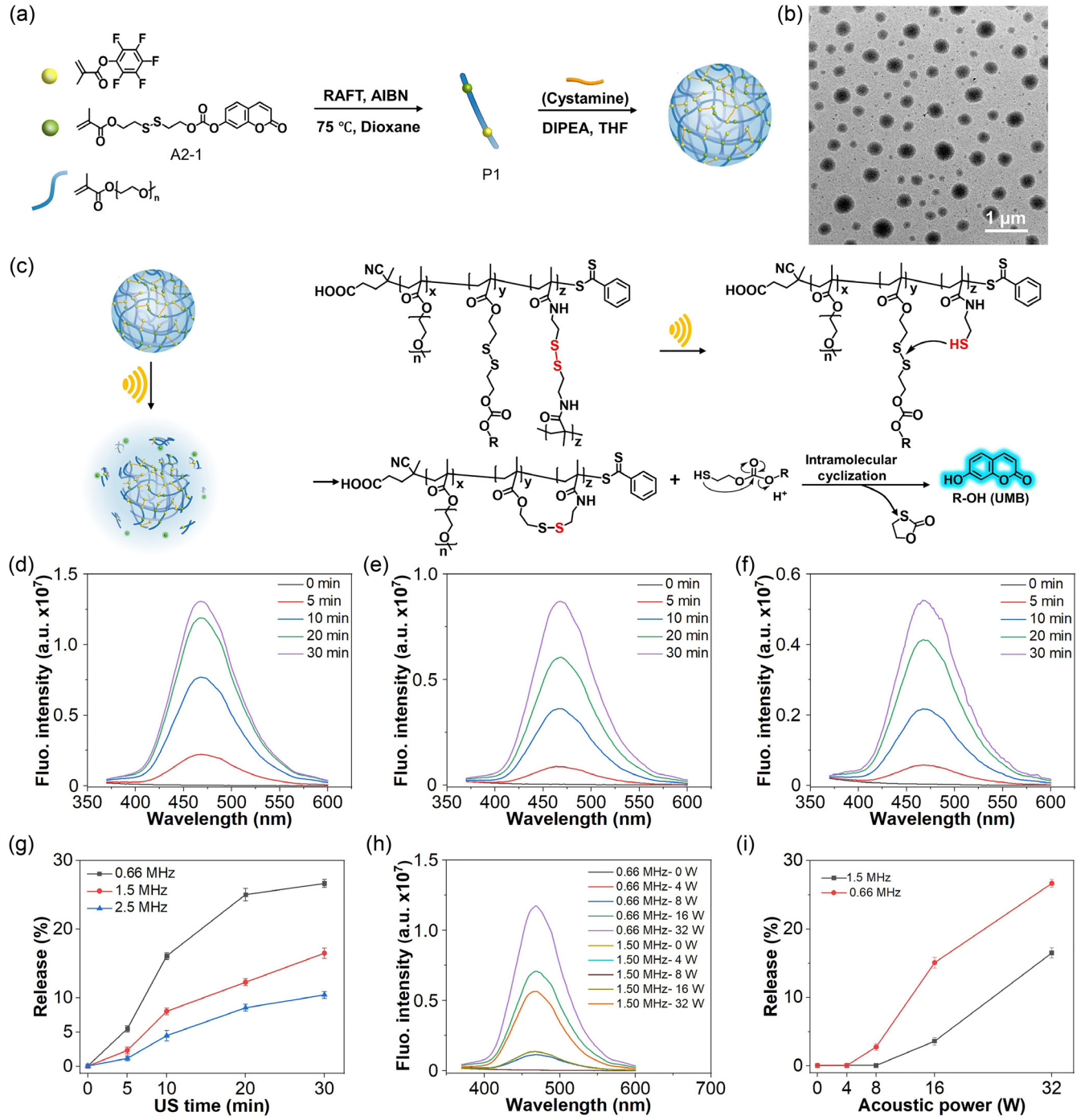


Figure 4 | *Synthesis and characterization of MGLs-UMB and HIFU activation of disulfide mechanophore in MGLs-UMB. (a) The synthesis of copolymer (P1) using RAFT polymerization of PEGMEMA, PFPMA and* ***A2-1*** *and the following cross-linking by cystamine to form MGLs-UMB. (b) TEM micrograph of MGLs-UMB. (c) The mechanism of disulfide mechanophore activation in MGLs-UMB. Fluorescence spectra of MGLs-UMB samples after (d) 0.66 MHz, (e) 1.5 MHz, and (f) 2.5 MHz HIFU treatment with an acoustic power of 32 W. (g) The release profile of UMB under HIFU treatment with different frequencies. (h) Fluorescence spectra of MGLs after 30 min HIFU sonication at different acoustic power. (i) UMB release from MGLs-UMB with different HIFU frequencies and acoustic power.*

DOI: 10.31635/ccschem.024.202403876
Citation: *CCS Chem.* **2024**, 6, 1895–1907
Link to VoR: https://doi.org/10.31635/ccschem.024.202403876

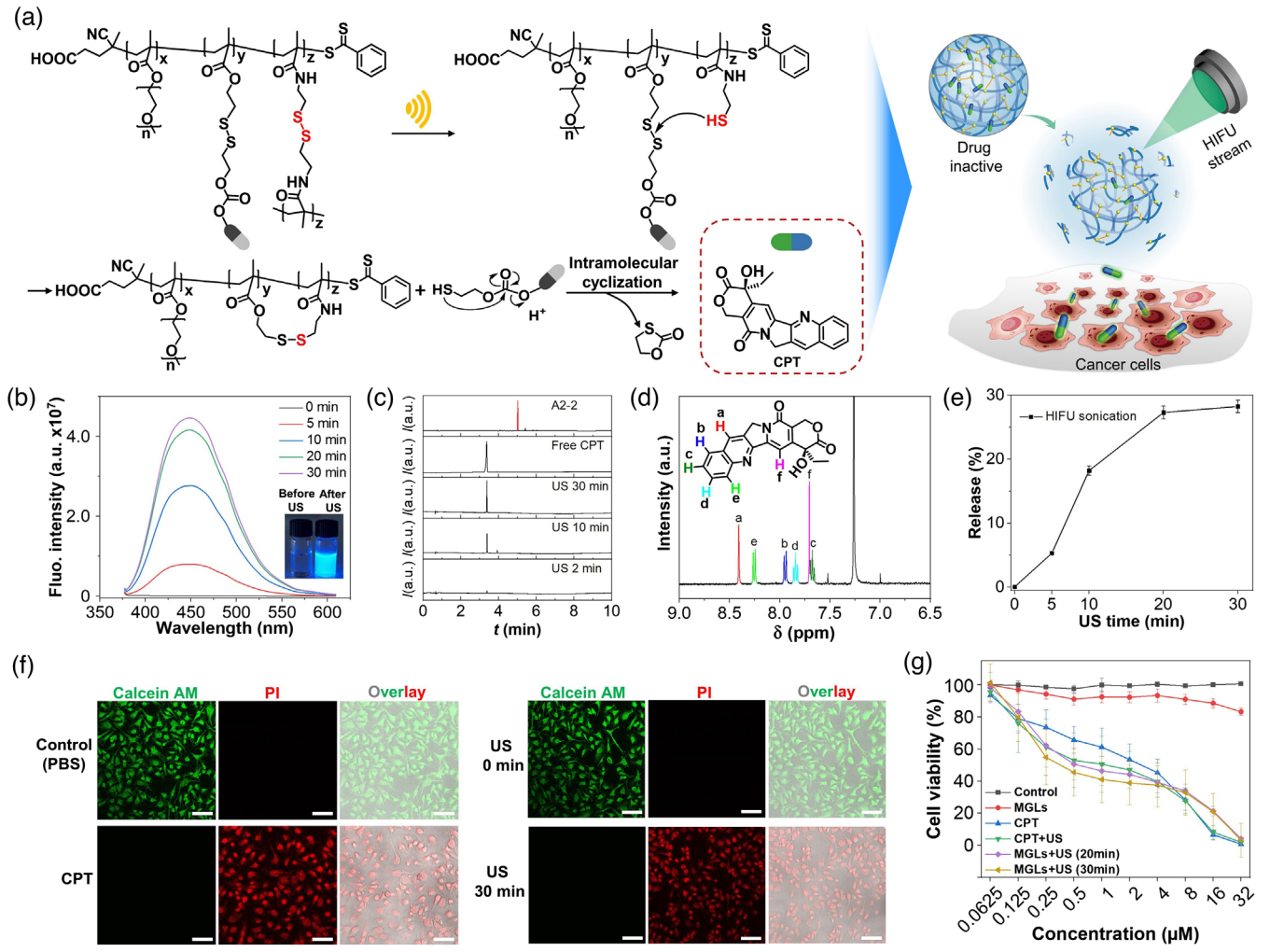


Figure 5 | *HIFU-induced disulfide mechanophore activation and model drug CPT release from MGLs. (a) Schematic illustration of disulfide mechanophore activation in MGLs-CPT and the subsequent CPT release for in vitro cancer therapy. (b) Fluorescence spectra of MGLs-CPT after HIFU treatment (0.66 MHz, 32 W). Inset is the image of MGLs-CPT solution under 365 nm UV illumination before and after HIFU treatment. (c) UPLC elugrams of A2-2, free CPT, and released CPT after HIFU treatment. (d) Section from ^{1}H NMR spectrum of released CPT (400 MHz, $CDCl_3$). Color-coded signals indicate the characteristic peaks of CPT. (e) The release profile of CPT from MGLs-CPT. (f) CLSM images of HeLa cells treated with different conditions (live cells: Calcein-AM, green; dead cells: PI, red). (1) PBS. (2) CPT. (3) Nonsonicated MGLs-CPT. (4) Sonicated MGLs-CPT (0.66 MHz, 30 min). HeLa cells were stained for 5 min. Scale bars: 50 μm. (g) Investigation of cell viability using MTS proliferation assay. Control (PBS), MGLs-CPT, CPT, CPT+US, and ex situ sonicated (0.66 MHz; 20 min or 30 min) MGLs-CPT mixed with HeLa cells. Mean values ± SD from the mean.* N = *3 independent HIFU experiments (Supporting Information Table S4).*

The mechanism of disulfide mechanophore activation and UMB release from MGLs-UMB under HIFU irradiation is illustrated in Figure 4c. Initially, 0.66 MHz HIFU was used to activate the disulfide mechanophores, as confirmed by fluorescence measurements (Figure 4d). Subsequently, 1.5 and 2.5 MHz HIFU were employed to test the response of MGLs. Both frequencies were able to trigger UMB release (Figure 4e,f). However, with 0.66 MHz HIFU, more disulfide mechanophores were activated, as indicated by higher fluorescence intensity compared to 1.5 and 2.5 MHz. The quantification of UMB release was assessed by using the approach described above in LPs and HBSPs (Supporting Information Figure S26), and it was observed that UMB release reached its maximum (~27%) after 20 min of sonication under 0.66 MHz HIFU treatment (Figure 4g). Moreover, the activation of disulfide mechanophores was almost completed within 30 min under 0.66 MHz irradiation, indicating that MGLs-UMB was more responsive to HIFU irradiation than LPs. TEM characterization of MGLs-UMB after 30 min of HIFU treatment revealed severe deformation and disintegration of the structure (Supporting

DOI: 10.31635/ccschem.024.202403876
Citation: *CCS Chem.* **2024**, 6, 1895–1907
Link to VoR: https://doi.org/10.31635/ccschem.024.202403876

Information Figure S27). From the bimodal size distribution histogram, we know that MGLs-UMB size increases with many small fragments occurring as well (Supporting Information Figure S28). However, not all MGLs-UMB were destroyed into smaller fragments. This phenomenon may be due to two reasons. First, the density of the cross-linked network is higher in the core part of the MGLs-UMB compared to the outer layer. During HIFU treatment, the mechanical forces caused by the US waves peeled off the corona layer from the surface of MGLs-UMB, leaving behind only the core parts.[45,50] Second, HIFU activation of the disulfide mechanophores in MGLs-UMB resulted in a reduction in cross-link density, causing the MGLs to lose their previous tight connections. This reduction in cross-link density led to structural swelling, which may have contributed to the retention of large-scale structures even after disintegration.

The relationship between HIFU power and UMB release from MGLs-UMB was investigated using 0.66 and 1.5 MHz HIFU frequencies since they exhibited higher disulfide mechanophore activation in MGLs-UMB. The fluorescence spectra of MGLs were measured after subjecting them to 30 min of HIFU sonication at different acoustic powers of 0, 4, 8, 16, and 32 W (Figure 4h). The results confirmed a positive relationship between fluorescence intensity and HIFU power. However, no fluorescence was detected when the HIFU acoustic power was lower than 4 W, indicating no activation of disulfide mechanophore in MGLs-UMB at lower HIFU power (Figure 4i). Therefore, the threshold value of HIFU acoustic power required to activate disulfide mechanophores for UMB release from MGLs-UMB was approximately 8 W when using the 0.66 MHz transducer.

HIFU-induced disulfide mechanophore activation in MGLs for drug release

After successfully demonstrating the release of UMB from different polymeric architectures, we expanded our investigation to incorporate a drug molecule, specifically CPT. CPT has shown promising anticancer activity in preliminary clinical trials, particularly against breast, colon, and stomach cancers.[51] However, CPT has low solubility in aqueous medium and can exhibit systemic toxicity.[52] To address these challenges, we aimed to achieve the spatiotemporally controlled release of CPT using our system. Therefore, MGLs-CPT was synthesized by cross-linking copolymers (20.8 kDa) with cystamine, which contains a disulfide mechanophore (Supporting Information Scheme S6 and Figure S29). In brief, CPT was covalently connected to the MGL chains through the acrylate molecule **A2-2**. The molar ratio of PEGMEMA to PFPMA to **A2-2** was approximately 17:4:1, and each P2 copolymer contained approximately three acrylate-CPT (**A2-2**) molecules (Supporting Information Figure S30). Subsequently, P2 was cross-linked using cystamine to obtain 70% (respect to the PFPMA moieties) cross-linked MGL-CPT. The morphology of MGL-CPT was analyzed using TEM (Supporting Information Figure S31).

To investigate the release of CPT from MGLs-CPT upon HIFU irradiation (Figure 5a), MGLs-CPT was dispersed in a solvent mixture of DMSO and PBS (v/v = 1:4) and then subjected to HIFU irradiation for 0, 5, 10, 20, and 30 min. The solution was subsequently filtered, and fluorescence spectra were measured to qualitatively assess the release of CPT from MGLs. The fluorescence spectra of CPT were collected with an excitation wavelength of 335 nm, showing a proportional relationship between fluorescence intensity and HIFU irradiation time (Figure 5b). Under UV illumination, a strong blue fluorescence was observed (Figure 5b inset). To further confirm these results, UPLC-MS analysis was employed to detect the appearance of CPT as a function of HIFU time (Figure 5c and Supporting Information Figure S32). Additionally, ^{1}H NMR analysis demonstrated the emergence of characteristic aromatic protons of CPT, providing clear evidence of HIFU-induced disulfide mechanophore activation and CPT release (Figure 5d). To quantify the amount released, a correlation between fluorescence intensity and CPT concentration was established (Supporting Information Figure S33). MCE was utilized to reduce all disulfide bonds within MGLs-CPT, and the maximum release was determined based on the fluorescence intensity (Supporting Information Figure S34). The treatment of MGLs-CPT with HIFU irradiation resulted in a maximum release of CPT of nearly 30%, and the release process reached a plateau after 20 min (Figure 5e and Supporting Information Figure S35).

To evaluate the potential of MGLs-CPT for in vitro treatment, we conducted experiments to assess its performance in delivering the drug to cancer cells. Confocal laser scanning microscopy (CLSM) and MTS proliferation assay were employed for this purpose. HeLa cells were treated under different conditions, including PBS, CPT alone, nonsonicated MGLs-CPT, and sonicated MGLs-CPT. Using CLSM, live cells were stained with calcein AM, while dead cells were stained with PI. The number of live HeLa cells significantly decreased when treated with the sample of sonicated MGLs-CPT for 30 min, with a death rate close to 100% (Figure 5f). Additionally, the mixture of MGLs-CPT with 20 min of sonication effectively inhibited the growth of HeLa cells (Supporting Information Figure S36). In comparison, neither PBS nor nonsonicated MGLs-CPT had a significant impact on the survival of HeLa cells.

Furthermore, the half-maximal inhibitory concentration (IC_{50}) of PBS, CPT alone, CPT applied with HIFU (0.66 MHz, 30 min), nonsonicated MGLs-CPT, and sonicated MGLs-CPT (0.66 MHz, 20 min or 30 min) was investigated. In the case of MGLs-CPT, the samples were subjected to HIFU irradiation ex situ before being added to the cell culture medium and incubated with HeLa cells.

DOI: 10.31635/ccschem.024.202403876
Citation: *CCS Chem.* **2024**, 6, 1895–1907
Link to VoR: https://doi.org/10.31635/ccschem.024.202403876

The IC_{50} values obtained after treating HeLa cells with PBS, CPT, CPT with sonication, nonsonicated MGLs-CPT, and sonicated MGLs-CPT were analyzed (Figure 5g and Supporting Information Table S4). We observed that the IC_{50} of sonicated MGLs-CPT was significantly lower compared to the control samples. The control samples, including PBS, showed no cytotoxic effect under the applied conditions. Cells treated with different concentrations of nonsonicated MGL samples exhibited high viability, indicating that MGLs had extremely low cell toxicity, possibly due to the good biocompatibility of the PEG chains. These results demonstrate the successful HIFU-induced mechanochemical disulfide activation and drug release in MGLs-CPS for sonopharmacology.

The activation efficiency of disulfide mechanophores in MGLs depended on the cross-link density and size of the MGLs (Supporting Information Figures S24 and S25). With 70% cross-linked MGLs-UMB (with respect to the PFPMA moieties), the release of UMB was 25% while in 100% cross-linked MGLs-UMB less than 5% was achieved as shown in Supporting Information Figure S37. The high cross-link density in MGLs contributes to high stability, potentially preventing the corona layer from chain solvation and thereby efficiently interacting with flow fields in the surrounding medium. Notably, extremely little activation of disulfide mechanophores was observed in smaller (50 nm) MGLs-UMB (Supporting Information Figure S37), suggesting that the size of polymer colloids also played a role for mechanophore activation. Our previous research has demonstrated that 200 nm MGLs are highly responsive to low-frequency sonication, with 20 kHz sonication treatment, triggering up to more than 60% released amount.[30] This suggests that MGLs of several hundred nanometers in size require strong cavitation to activate mechanophores and explains why 0.66 MHz sonication exhibits superior mechanophore activation efficiency compared to 1.5 or 2.5 MHz irradiation treatment; the lower frequency results in stronger cavitation at a similar power intensity. In addition, the MI can be consulted as a measure of cavitation bioeffects.[53,54] Currently, the United States Food and Drug Administration stipulates that diagnostic US scanners are safe with a MI below 1.9. Hence, in our polymeric nanomaterials system, 0.66 MHz transducer with an 8 W acoustic power was chosen for the drug release assay due to its relatively low MI of 1.5.

In the case of HBSPs, the threshold of acoustic power for mechanophore activation was 4 W and was lower than the one in MGLs (8 W). It might be that the unique star-shape architecture results in high force transduction efficiency. Notably, in HBSPs the best activation frequency was 1.5 MHz compared to 0.66 MHz for MGLs, suggesting that a factor other than cavitation might contribute to the activation of mechanophores. However, this requires further investigation and will be addressed in future research.

Conclusion

In summary, our study has demonstrated the activation of disulfide mechanophores in different polymeric nanostructures, HBSPs and MGLs, through HIFU, leading to the release of target molecules including fluorophores and active pharmaceutical ingredients via disulfide exchange and subsequent cleavage of a carbonate linker. The structures of HBSPs and MGLs were characterized using TEM, and the activation of disulfide mechanophores and molecular release were confirmed through ESI mass and UPLC measurements. Fluorescence measurements allowed for the quantification of molecular release under different HIFU parameters, including frequency, power, and time. Furthermore, an in vitro study of drug release was carried out using the MGLs-CPT system, and the efficacy of released CPT was evaluated using CLSM and MTS proliferation assays. A unique feature of the current system is the utilization of HIFU as a stimulus similar to what is used in medical applications, which represents an important step for exploiting polymer mechanochemistry in the field of biomedicine. Moreover, considering the presence of different kinds of mechanophores and the fact that thiol groups can initiate various chemical reactions, this work provides further insights into the design of new drug delivery and release systems based on polymer mechanochemistry using MHz HIFU modalities.

Supporting Information

Supporting Information is available and includes additional experimental details (synthetic procedures and characterization data; polymerization procedures and polymer analysis; supporting fluorescence spectra, GPC spectra, MTS proliferation assays, CLSM, DLS data, TEM images, and HIFU parameters).

Conflict of Interest

There are no conflicts of interest to report.

Funding Information

This work was financially supported by the German Research Foundation (grant nos. 331065168, 191948804, and 503981124). L.Z. acknowledges funding from the National Natural Science Foundation of China (grant no. 22277018), the Zhejiang Provincial Natural Science Foundation for Distinguished Young Scholars (grant no. LR23B030001), and Wenzhou Institute, University of the Chinese Academy of Sciences (grant no. WIUCASQD2020015). M.X. acknowledges the financial support of the Alexander von Humboldt Foundation (grant no. 3.5-CHN-1210658-HFST-P).

DOI: 10.31635/ccschem.024.202403876
Citation: *CCS Chem.* **2024**, 6, 1895–1907
Link to VoR: https://doi.org/10.31635/ccschem.024.202403876

References

1. Davis, D. A.; Hamilton, A.; Yang, J.; Cremar, L. D.; Van Gough, D.; Potisek, S. L.; Ong, M. T.; Braun, P. V.; Martínez, T. J.; White, S. R.; Moore, J. S.; Sottos, N. R. Force-Induced Activation of Covalent Bonds in Mechanoresponsive Polymeric Materials. *Nature* **2009**, *459*, 68–72.
2. Lenhardt, J. M.; Ong, M. T.; Choe, R.; Evenhuis, C. R.; Martinez, T. J.; Craig, S. L. Trapping a Diradical Transition State by Mechanochemical Polymer Extension. *Science* **2010**, *329*, 1057–1060.
3. Chen, Z.; Mercer, J. A. M.; Zhu, X.; Romaniuk, J. A. H.; Pfattner, R.; Cegelski, L.; Martinez, T. J.; Burns, N. Z.; Xia, Y. Mechanochemical Unzipping of Insulating Polyladderene to Semiconducting Polyacetylene. *Science* **2017**, *357*, 475–479.
4. Overholts, A. C.; Granados Razo, W.; Robb, M. J. Mechanically Gated Formation of Donor–Acceptor Stenhouse Adducts Enabling Mechanochemical Multicolour Soft Lithography. *Nat. Chem.* **2023**, *15*, 332–338.
5. Shen, H.; Larsen, M. B.; Roessler, A. G.; Zimmerman, P. M.; Boydston, A. J. Mechanochemical Release of N-Heterocyclic Carbenes from Flex-Activated Mechanophores. *Angew. Chem. Int. Ed.* **2021**, *60*, 13559–13563.
6. Lenhardt, J. M.; Black, A. L.; Craig, S. L. Gem-Dichlorocyclopropanes as Abundant and Efficient Mechanophores in Polybutadiene Copolymers Under Mechanical Stress. *J. Am. Chem. Soc.* **2009**, *131*, 10818–10819.
7. Hu, X.; Zeng, T.; Husic, C. C.; Robb, M. J. Mechanically Triggered Small Molecule Release from a Masked Furfuryl Carbonate. *J. Am. Chem. Soc.* **2019**, *141*, 15018–15023.
8. Li, Y.; Nese, A.; Matyjaszewski, K.; Sheiko, S. S. Molecular Tensile Machines: Anti-Arrhenius Cleavage of Disulfide Bonds. *Macromolecules* **2013**, *46*, 7196–7201.
9. Hemmer, J. R.; Rader, C.; Wilts, B. D.; Weder, C.; Berrocal, J. A. Heterolytic Bond Cleavage in a Scissile Triarylmethane Mechanophore. *J. Am. Chem. Soc.* **2021**, *143*, 18859–18863.
10. Sagara, Y.; Karman, M.; Verde-Sesto, E.; Matsuo, K.; Kim, Y.; Tamaoki, N.; Weder, C. Rotaxanes as Mechanochromic Fluorescent Force Transducers in Polymers. *J. Am. Chem. Soc.* **2018**, *140*, 1584–1587.
11. Konda, S. S. M.; Brantley, J. N.; Varghese, B. T.; Wiggins, K. M.; Bielawski, C. W.; Makarov, D. E. Molecular Catch Bonds and the Anti-Hammond Effect in Polymer Mechanochemistry. *J. Am. Chem. Soc.* **2013**, *135*, 12722–12729.
12. Chen, Y.; Spiering, A. J. H.; Karthikeyan, S.; Peters, G. W. M.; Meijer, E. W.; Sijbesma, R. P. Mechanically Induced Chemiluminescence from Polymers Incorporating a 1,2-Dioxetane Unit in the Main Chain. *Nat. Chem.* **2012**, *4*, 559–562.
13. Larsen, M. B.; Boydston, A. J. "Flex-Activated" Mechanophores: Using Polymer Mechanochemistry to Direct Bond Bending Activation. *J. Am. Chem. Soc.* **2013**, *135*, 8189–8192.
14. Nixon, R.; De Bo, G. Isotope Effect in the Activation of a Mechanophore. *J. Am. Chem. Soc.* **2021**, *143*, 3033–3036.
15. Li, J.; Shiraki, T.; Hu, B.; Wright, R. A. E.; Zhao, B.; Moore, J. S. Mechanophore Activation at Heterointerfaces. *J. Am. Chem. Soc.* **2014**, *136*, 15925–15928.
16. Church, D. C.; Peterson, G. I.; Boydston, A. J. Comparison of Mechanochemical Chain Scission Rates for Linear Versus Three-Arm Star Polymers in Strong Acoustic Fields. *ACS Macro Lett.* **2014**, *3*, 648–651.
17. Zhang, Y.; Lund, E.; Gossweiler, G. R.; Lee, B.; Niu, Z.; Khripin, C.; Munch, E.; Couty, M.; Craig, S. L. Molecular Damage Detection in an Elastomer Nanocomposite with a Coumarin Dimer Mechanophore. *Macromol. Rapid Commun.* **2021**, *42*, 2000359.
18. Clough, J. M.; van der Gucht, J.; Sijbesma, R. P. Mechanoluminescent Imaging of Osmotic Stress-Induced Damage in a Glassy Polymer Network. *Macromolecules* **2017**, *50*, 2043–2053.
19. Nofen, E. M.; Zimmer, N.; Dasgupta, A.; Gunckel, R.; Koo, B.; Chattopadhyay, A.; Dai, L. L. Stress-Sensing Thermoset Polymer Networks via Grafted Cinnamoyl/Cyclobutane Mechanophore Units in Epoxy. *Polym. Chem.* **2016**, *7*, 7249–7259.
20. Chen, Y.; Yeh, C. J.; Guo, Q.; Qi, Y.; Long, R.; Creton, C. Fast Reversible Isomerization of Merocyanine as a Tool to Quantify Stress History in Elastomers. *Chem. Sci.* **2021**, *12*, 1693–1701.
21. Qian, H.; Purwanto, N. S.; Ivanoff, D. G.; Halmes, A. J.; Sottos, N. R.; Moore, J. S. Fast, Reversible Mechanochromism of Regioisomeric Oxazine Mechanophores: Developing in Situ Responsive Force Probes for Polymeric Materials. *Chem* **2021**, *7*, 1080–1091.
22. Chen, Z.; Ye, F.; Shao, T.; Wu, Y.; Chen, M.; Zhang, Y.; Zhao, X.; Zou, B.; Ma, Y. Stress-Dependent Multicolor Mechanochromism in Epoxy Thermosets Based on Rhodamine and Diaminodiphenylmethane Mechanophores. *Macromolecules* **2022**, *55*, 2310–2319.
23. Sulkanen, A. R.; Sung, J.; Robb, M. J.; Moore, J. S.; Sottos, N. R.; Liu, G. Spatially Selective and Density-Controlled Activation of Interfacial Mechanophores. *J. Am. Chem. Soc.* **2019**, *141*, 4080–4085.
24. Shi, Z.; Wu, J.; Song, Q.; Göstl, R.; Herrmann, A. Toward Drug Release Using Polymer Mechanochemical Disulfide Scission. *J. Am. Chem. Soc.* **2020**, *142*, 14725–14732.
25. Huo, S.; Zhao, P.; Shi, Z.; Zou, M.; Yang, X.; Warszawik, E.; Loznik, M.; Göstl, R.; Herrmann, A. Mechanochemical Bond Scission for the Activation of Drugs. *Nat. Chem.* **2021**, *13*, 131–139.
26. Shi, Z.; Song, Q.; Göstl, R.; Herrmann, A. Mechanochemical Activation of Disulfide-Based Multifunctional Polymers for Theranostic Drug Release. *Chem. Sci.* **2021**, *12*, 1668–1674.
27. Shi, Z.; Song, Q.; Göstl, R.; Herrmann, A. The Mechanochemical Release of Naphthalimide Fluorophores from β-Carbonate and β-Carbamate Disulfide-Centered Polymers. *CCS Chem.* **2021**, *3*, 2333–2344.
28. Huo, S.; Liao, Z.; Zhao, P.; Zhou, Y.; Göstl, R.; Herrmann, A. Mechano-Nanoswitches for Ultrasound-Controlled Drug Activation. *Adv. Sci.* **2022**, *9*, 2104696.

DOI: 10.31635/ccschem.024.202403876
Citation: *CCS Chem.* **2024**, 6, 1895–1907
Link to VoR: https://doi.org/10.31635/ccschem.024.202403876

29. Zou, M.; Zhao, P.; Huo, S.; Göstl, R.; Herrmann, A. Activation of Antibiotic-Grafted Polymer Brushes by Ultrasound. *ACS Macro Lett.* **2022**, *11*, 15–19.
30. Zou, M.; Zhao, P.; Fan, J.; Göstl, R.; Herrmann, A. Microgels as Drug Carriers for Sonopharmacology. *J. Polym. Sci.* **2022**, *60*, 1864–1870.
31. Kim, G.; Lau, V. M.; Halmes, A. J.; Oelze, M. L.; Moore, J. S.; Li, K. C. High-Intensity Focused Ultrasound-Induced Mechanochemical Transduction in Synthetic Elastomers. *Proc. Natl. Acad. Sci. USA* **2019**, *116*, 10214–10222.
32. Kim, G.; Wu, Q.; Chu, J. L.; Smith, E. J.; Oelze, M. L.; Moore, J. S.; Li, K. C. Ultrasound Controlled Mechanophore Activation in Hydrogels for Cancer Therapy. *Proc. Natl. Acad. Sci. U. S. A.* **2022**, *119*, e2109791119.
33. Yao, Y.; McFadden, M. E.; Luo, S. M.; Barber, R. W.; Kang, E.; Bar-Zion, A.; Smith, C. A. B.; Jin, Z.; Legendre, M.; Ling, B.; Malounda, D.; Torres, A.; Hamza, T.; Edwards, C. E. R.; Shapiro, M. G.; Robb, M. J. Remote Control of Mechanochemical Reactions under Physiological Conditions Using Biocompatible Focused Ultrasound. *Proc. Natl. Acad. Sci. USA* **2023**, *120*, e2309822120.
34. Yildiz, D.; Göstl, R.; Herrmann, A. Sonopharmacology: Controlling Pharmacotherapy and Diagnosis by Ultrasound-Induced Polymer Mechanochemistry. *Chem. Sci.* **2022**, *13*, 13708–13719.
35. Küng, R.; Göstl, R.; Schmidt, B. M. Release of Molecular Cargo from Polymer Systems by Mechanochemistry. *Chem. Eur. J.* **2022**, *28*, e202103860.
36. Versaw, B. A.; Zeng, T.; Hu, X.; Robb, M. J. Harnessing the Power of Force: Development of Mechanophores for Molecular Release. *J. Am. Chem. Soc.* **2021**, *143*, 21461–21473.
37. Mitragotri, S. Healing Sound: The Use of Ultrasound in Drug Delivery and Other Therapeutic Applications. *Nat. Rev. Drug Discov.* **2005**, *4*, 255–260.
38. Phenix, C. P.; Togtema, M.; Pichardo, S.; Zehbe, I.; Curiel, L. High Intensity Focused Ultrasound Technology, Its Scope and Applications in Therapy and Drug Delivery. *J. Pharm. Pharm. Sci.* **2014**, *17*, 136–153.
39. Park, I.; Sheiko, S. S.; Nese, A.; Matyjaszewski, K. Molecular Tensile Testing Machines: Breaking a Specific Covalent Bond by Adsorption-Induced Tension in Brushlike Macromolecules. *Macromolecules* **2009**, *42*, 1805–1807.
40. Kucharski, T. J.; Huang, Z.; Yang, Q.-Z.; Tian, Y.; Rubin, N. C.; Concepcion, C. D.; Boulatov, R. Kinetics of Thiol/Disulfide Exchange Correlate Weakly with the Restoring Force in the Disulfide Moiety. *Angew. Chem. Int. Ed.* **2009**, *48*, 7040–7043.
41. Fritze, U. F.; von Delius, M. Dynamic Disulfide Metathesis Induced by Ultrasound. *Chem. Commun.* **2016**, *52*, 6363–6366.
42. Wang, F.; Burck, M.; Diesendruck, C. E. Following Homolytic Mechanochemical Kinetics with a Pyrenyl Nitrone Spin Trap. *ACS Macro Lett.* **2017**, *6*, 42–45.
43. Fritze, U. F.; Craig, S. L.; von Delius, M. Disulfide-Centered Poly(Methyl Acrylates): Four Different Stimuli to Cleave a Polymer. *J. Polym. Sci. A Polym. Chem.* **2018**, *56*, 1404–1411.
44. Kida, J.; Aoki, D.; Otsuka, H. Self-Strengthening of Cross-Linked Elastomers via the Use of Dynamic Covalent Macrocyclic Mechanophores. *ACS Macro Lett.* **2021**, *10*, 558–563.
45. Schulte, M. F.; Izak-Nau, E.; Braun, S.; Pich, A.; Richtering, W.; Göstl, R. Microgels React to Force: Mechanical Properties, Syntheses, and Force-Activated Functions. *Chem. Soc. Rev.* **2022**, *51*, 2939–2956.
46. May, P. A.; Munaretto, N. F.; Hamoy, M. B.; Robb, M. J.; Moore, J. S. Is Molecular Weight or Degree of Polymerization a Better Descriptor of Ultrasound-Induced Mechanochemical Transduction? *ACS Macro Lett.* **2016**, *5*, 177–180.
47. Schaefer, M.; Icli, B.; Weder, C.; Lattuada, M.; Kilbinger, A. F. M.; Simon, Y. C. The Role of Mass and Length in the Sonochemistry of Polymers. *Macromolecules* **2016**, *49*, 1630–1636.
48. Malhotra, S. L. Ultrasonic Solution Degradations of Poly(Alkyl Methacrylates). *J. Macromol. Sci. A – Chem.* **1986**, *23*, 729–748.
49. Kryger, M. J.; Munaretto, A. M.; Moore, J. S. Structure–Mechanochemical Activity Relationships for Cyclobutane Mechanophores. *J. Am. Chem. Soc.* **2011**, *133*, 18992–18998.
50. Izak-Nau, E.; Demco, D. E.; Braun, S.; Baumann, C.; Pich, A.; Göstl, R. Shear-Induced Structural and Functional Transformations of Poly(N-Vinylcaprolactam) Microgels. *ACS Appl. Polym. Mater.* **2020**, *2*, 1682–1691.
51. Wang, X. H.; Huang, M.; Zhao, C. K.; Li, C.; Xu, L. Design, Synthesis, and Biological Activity Evaluation of Camptothecin-HAA-Norcantharidin Conjugates as Antitumor Agents in Vitro. *Chem. Biol. Drug. Des.* **2019**, *93*, 986–992.
52. Krishnan, P.; Rajan, M.; Kumari, S.; Sakinah, S.; Priya, S. P.; Amira, F.; Danjuma, L.; Pooi Ling, M.; Fakurazi, S.; Arulselvan, P.; Higuchi, A.; Arumugam, R.; Alarfaj, A. A.; Munusamy, M. A.; Hamat, R. A.; Benelli, G.; Murugan, K.; Kumar, S. S. Efficiency of Newly Formulated Camptothecin with β-Cyclodextrin-EDTA-Fe_3O_4 Nanoparticle-Conjugated Nanocarriers as an Anti-Colon Cancer (HT29) Drug. *Sci. Rep.* **2017**, *7*, 10962.
53. Apfel, R. E.; Holland, C. K. Gauging the Likelihood of Cavitation from Short-Pulse, Low-Duty Cycle Diagnostic Ultrasound. *Ultrasound Med. Biol.* **1991**, *17*, 179–185.
54. Church, C. C.; Labuda, C.; Nightingale, K. A Theoretical Study of Inertial Cavitation from Acoustic Radiation Force Impulse Imaging and Implications for the Mechanical Index. *Ultrasound Med. Biol.* **2015**, *41*, 472–485.

DOI: 10.31635/ccschem.024.202403876
Citation: *CCS Chem.* **2024**, 6, 1895–1907
Link to VoR: https://doi.org/10.31635/ccschem.024.202403876